Dalton Transactions

ROYAL SOCIETY OF CHEMISTRY

PAPER

View Article Online
View Journal | View Issue

Cite this: *Dalton Trans.*, 2020, **49**, 923

The effect of the layer-interlayer chemistry of LDHs on developing high temperature carbon capture materials†

G. V. Manohara, * M. Mercedes Maroto-Valer and Susana Garcia*

Received 3rd October 2019,
Accepted 3rd December 2019

DOI: 10.1039/c9dt03913a

rsc.li/dalton

The layer-interlayer chemistry of layered double hydroxides (LDHs) offers a vast opportunity to develop mixed metal oxides (MMOs) as novel sorbents for high temperature CO_2 capture. Here, we report the synthesis of adamantanecarboxylate intercalated Ca–Al LDH by employing a co-hydration method. Thermal decomposition under a controlled atmosphere converts the layered metal hydroxides to MMOs and an intercalated anion into a carbonaceous support. The higher thermal stability and polymeric nature of the intercalated adamantanecarboxylate ion act as a thermal/mechanical support for the layered MMOs. The resultant hybrid solid sorbent shows excellent high temperature CO_2 capture and cycling performance under both CO_2 rich and lean (industrial flue gas) conditions. The hybrid sample shows almost 100% carbonation of all the active phase present, leading to maximum atom efficiency. The hybrid sorbent also shows rapid kinetics for both the carbonation and regeneration steps. The employed synthetic strategy offers a new approach to develop improved novel sorbents based on LDHs for high temperature CO_2 capture.

1. Introduction

The role of CO_2 on global warming and its consequences is well known.[1,2] Significant efforts have been made to move away from fossil fuels for energy dependency and to capture and store the emitted carbon dioxide.[3,4] Carbon dioxide capture and storage (CCS),[5] and carbon dioxide capture and utilization (CCU) are two main themes employed to address the challenge of CO_2 emissions and its consequences.[6]

At present, "amine scrubbing" involving an absorption process using liquid amines such as monoethanolamine to capture CO_2 is currently taking place on an industrial scale.[7] For greater economic and environmental sustainability, the use of liquid amines to capture CO_2 is not promising for various reasons: (a) there is a large energy penalty for regeneration, (b) a temperature limit of operation, and (c) toxic by-products during the regeneration of amines and so on.[8] To overcome the limitations of liquid solvents and to lower the cost of the capture process, solid sorbents for CO_2 capture are gaining importance. Porous carbon, zeolites, metal–organic frameworks (MOFs), covalent organic frameworks (COFs), metal oxides, mixed metal oxides (MMOs) based on layered double hydroxides (LDHs), perovskites, lithium-based ceramics and oxides of calcium are some of the solid sorbents studied for CO_2 capture.[9] Although solid sorbents have gained a lot of attention and there is steady progress with the promise to replace liquid amines on the industrial scale,[10] most of these solid sorbents have limited operating temperatures for capture (generally <100 °C).[11] Moreover, there is a need to focus on solid sorbents that operate at industrial flue gas emission temperatures (200–800 °C) such as those used in the cement, oil refinery, iron and steel industries.[12] Metal oxides, mixed metal oxides and alkali metal ceramics show promising CO_2 capture behaviour (0.5 to 16 mmol g^{-1}) under flue gas conditions.[13] However, the progress on this kind of medium to high temperature solid sorbents is rather slow or limited compared to that of other types of solid sorbents. Physisorbents such as MOFs, COFs, zeolites and porous carbon-based materials show good CO_2 capture and cycling stability at low temperatures (<100 °C).[9d] Other solid sorbents that work at medium to high temperatures (200–650 °C), such as CaO and alkali metal-based ceramics show good CO_2 capture capacities but lack long term cycling stability.[9b] On the other hand, LDH-based MMOs show poor capture and cycling stability. Therefore, this work focuses on the development of improved novel LDH-based solid sorbents that can successfully operate at high temperatures under industrial flue gas CO_2 concentrations.

LDH-based MMOs are ideal candidate materials for capturing CO_2 under industrial flue gas conditions due to their (a)

Research Centre for Carbon Solutions (RCCS), School of Engineering and Physical Sciences, Heriot-Watt University, Edinburgh EH14 4AS, UK.
E-mail: s.garcia@hw.ac.uk, manoharagv@gmail.com

†Electronic supplementary information (ESI) available. See DOI: 10.1039/c9dt03913a

fast adsorption/desorption kinetics, (b) ability to operate from medium to high temperatures (200–800 °C), (c) wide compositional variability that can be tuned to obtain a high CO_2 capture capacity, (d) tolerance to moisture, and (e) being environmentally benign and economical.[14] LDHs derive their structure from mineral brucite $Mg(OH)_2$ and are represented by the general formula $[M^{2+}_{1-x}M^{3+}_{x}(OH)_2]^{x+}(A^{-x/n})\cdot yH_2O$, where M^{2+} = Mg, Co, Ni, Ca or Zn, M^{3+} = Al, Fe or Ga, A = anion (organic or inorganic ions), $0.15 \leq x \leq 0.33$ and $0.5 \leq y \leq 1.0$.[15] LDHs show various physicochemical properties and have been used in a wide range of applications.[16] Thermal decomposition of LDHs generates MMOs that have basic characteristics.[17] These MMOs have gained a lot of attention as pre/post combustion CO_2 capture sorbents.[18] The basicity and porosity of these oxides can be tuned by varying the layered metal cations and interlayer anions.[19] These MMOs present a theoretically high CO_2 capture capacity (17 to 34 mmol g^{-1}, depending on the composition), which can be exploited at medium to high temperatures. Unfortunately, they still have several limitations, including a low measured capture capacity (around 1 mmol g^{-1}), poor thermal and mechanical stability and particle aggregation during cycling.[20] Although there have been some efforts towards addressing these issues using various approaches,[21] there has been no sufficient progress made to utilize these MMOs for large scale CO_2 capture.

It is very important to understand the crystal chemistry and physicochemical properties of LDHs to develop novel MMOs that show higher capture and a better cycling stability than those previously reported.[20] Thermal decomposition of LDHs leading to the formation of MMOs involves three different steps.[17] In the first step, the adsorbed water is eliminated followed by a second step where the removal of intercalated anions and crystalline water molecules occurs. This step removes the interlayer space between the metal hydroxide sheets. Finally, in the third step, the dehydroxylation of the layered hydroxides takes place, leading to the formation of the MMOs. However, during the thermal decomposition step, the LDHs lose their interlayer space and layered structure leading to the formation of agglomerated MMOs (Scheme 1). These two factors have contributed significantly to the poor CO_2 capture performance of LDH-based MMOs reported so far. Therefore, it is important to synthesize LDHs in such a way so that they retain/transform the interlayer anion as a stable support for the resultant MMOs during thermal decomposition.

Diamondoids and their derivatives are known to transform into diamond nanowires or linear carbon chains when confined in narrow galleries of carbon nanotubes.[22] Recently, adamantanecarboxylate intercalated LDH was converted into linear carbon chain/wire supported MMOs under controlled decomposition.[23] Herein, we employ a similar approach to synthesize a Ca–Al-adamantanecarboxylate intercalated LDH using only stoichiometric amounts (no excess chemicals used) of metal hydroxide (source of metal ions) and 1-adamantanecarboxylic acid (source of anion). The synthesized Ca–Al LDH was converted into a carbon-supported MMOs under an inert atmosphere. The resultant carbon supported MMOs was tested for high temperature carbon dioxide capture and cyclability under industrial flue gas CO_2 concentrations.

2. Experimental section

Synthesis of LDH and supported MMOs

All of the chemicals, $Ca(OH)_2$, $Al(OH)_3$ and 1-adamantanecarboxylic acid were purchased from Sigma Aldrich and were used as received. Deionised water (18 MΩ cm resistivity, Millipore water purification system) was used throughout the experiments. Adamantanecarboxylate intercalated with Ca–Al (Ca/Al = 2) was synthesized by employing a co-hydration method. In a typical experiment, stoichiometric amounts of $Ca(OH)_2$ (0.008 moles, 0.625g), $Al(OH)_3$ (0.004 moles, 0.328 g) and 1-adamantanecarboxylic acid (0.004 moles, 0.7579 g) (Al/adamantanecarboxylate = 1) were taken up in 100 mL of water. The reaction mixture was stirred at room temperature for an hour to obtain a homogeneous mixture. The resultant reaction mixture was transferred to a Teflon lined vessel and was hydrothermally treated at 110 °C for 24 h. The resultant LDH was recovered by filtration followed by drying at 65 °C overnight. The carbon-supported MMOs was synthesized by decomposing the Ca–Al-adamantanecarboxylate LDH under an inert N_2 atmosphere. In a typical experiment, 1 g of Ca–Al-adamantanecarboxylate LDH was loaded into a quartz tube and was subjected to decomposition at 700 °C under a N_2 atmosphere (N_2 [99.99% purity] flow rate of 100 mL min^{-1}, ramp rate 10 °C min^{-1}, residence time 2 h).

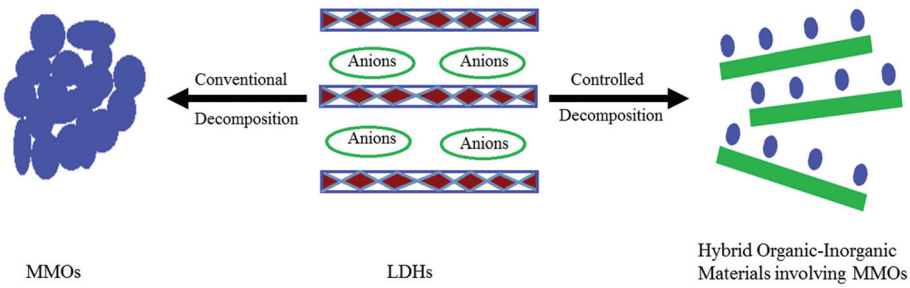

Scheme 1 Schematic representation of the thermal decomposition of LDHs by conventional and controlled methods.

Sample characterization

Powder X-ray diffraction (PXRD) patterns were recorded on a Bruker D8 Advance powder diffractometer, using Ge-monochromated Cu-Kα1 radiation (λ = 1.5406 Å) from a sealed tube, operating at 40 kV and 40 mA with a LynxEye linear detector in reflectance mode. Data was collected over an angular 2θ range of 5–85° with a step size of 0.009° over a one hour period. The Fourier-transform infrared spectra (FTIR) of the samples were measured using a PerkinElmer spectrometer in ATR mode (4000 to 400 cm^{-1}). Raman spectra were recorded with a Jobin Yvon Horiba LabRAM spectrometer using Nd:YAG (532 nm) laser excitation. Thermal analysis and CO_2 capture studies were performed using a thermogravimetric analyser (TA Instruments TA 500). Elemental analysis of Ca^{2+} and Al^{3+} (ICP-OES) was carried out by an atomic emission technique using a PerkinElmer Optima 5300DV. A mixture of concentrated nitric acid and hydrochloric acid in a ratio was used to dissolve the LDH. The solution was diluted 20 times prior to analysis. The C, H and N analysis of the LDH samples was carried out using approximately 3 mg of the sample and placing it in a tin capsule for combustion in a high oxygen environment at 950 °C using an Exeter Analytical CE-440 elemental analyser calibrated with acetanilide. Surface area analysis of the sample was carried out using a gas adsorption technique (N_2, 77 K) with a Micromeritics ASAP 2020 instrument. Prior to the gas adsorption measurements, the sample was degassed for 3 h at 150 °C. Transmission electron microscopy (TEM) and high-resolution TEM (HRTEM) images were acquired using a JEOL 2100F FEG TEM. The surface morphology of the sample was characterized by scanning electron microscopy (SEM) using an FEI Quanta FEG SEM.

CO_2 capture studies

Pristine Ca–Al-adamantanecarboxylate LDH was used instead of preformed MMOs to avoid CO_2 contamination. Freshly prepared LDH was loaded into a platinum pan and decomposed under an inert atmosphere (using 100 mL min^{-1} N_2 [99.99% purity], 2 h, 700 °C, 10 °C min^{-1}). Once the decomposition was complete, the temperature was brought back to the desired capture temperature and the CO_2 (99.98% purity) gas supply was switched on (for 2 h) to test the uptake capacity of the resultant MMOs. The cycling performance of the resultant MMOs was studied by conducting consecutive adsorption–desorption cycles at two different CO_2 concentrations (60 cycles at 86% CO_2 and 40 cycles at 14% CO_2). Adsorption cycles were performed at 600 °C for 30 min under a CO_2 atmosphere and desorption/regeneration was performed at 700 °C for 30 min under N_2. In a typical experiment, around 10 mg of the freshly prepared Ca–Al-adamantanecarboxylate LDH was placed in a platinum pan. The MMOs were first generated by decomposing the sample under a N_2 atmosphere at 700 °C for 2h (ramp 10 °C min^{-1}). After this step, the sample was brought back to the desired temperature (10 °C min^{-1}) under N_2 and the gas was switched to CO_2. The adsorption step was performed for 30 min under CO_2 and then the desorption step was carried out (30 min) by switching the gas to N_2 and increasing the temperature to 700 (10 °C min^{-1}).

3. Results and discussion

Conventionally, the MMOs derived from LDHs employed for CO_2 capture show negligible capture and poor cycling stability mainly due to (i) agglomeration of particles (during the thermal decomposition of LDHs to derive the MMOs) and (ii) poor thermal/mechanical stability of the MMOs.[20,21] Here we try to address these two issues by synthesizing Ca–Al-adamantanecarboxylate LDH and converting it into novel MMOs that have better CO_2 capture ability and cycling stability. The anion, adamantanecarboxylate, was chosen due to its better thermal stability and ability to transform into a carbon support under controlled decomposition. Upon controlled thermal decomposition, the layered metal hydroxides of the LDH are expected to convert to MMOs and the interlayer anion will provide support to the formed MMOs by converting itself to a carbonaceous residue.

Synthesis of Ca–Al LDH and its conversion into an organic–inorganic composite

The Ca/Al-adamantanecarboxylate (Ca/Al = 2) LDH sample was synthesized using the metal hydroxides $Ca(OH)_2$ and $Al(OH)_3$, and 1-adamantanecarboxylic acid by employing the co-hydration method.[24] The employed method is greener and more sustainable compared to the widely used co-precipitation or homogeneous precipitation from solution (HPFS) methods.[15] Here, only a stoichiometric amount of the metal hydroxides and carboxylic acid was used as a source of the metal ions and anions, respectively, as opposed to the large excess of chemicals used in the other methods. In addition, there is no post synthesis washing steps involved in the employed method, as there are no excess chemicals used and this will greatly reduce the amount of water required for the LDH synthesis.

The composition of the as-synthesized Ca–Al-adamantanecarboxylate intercalated LDH was calculated based on CHN and ICP analysis. CHN analysis data gave 30.4% C and 5.2% H, while ICP analysis data gave a Ca/Al molar ratio of 2.44. Based on the experimental Ca/Al ratio, and assuming minimal carbonate contamination, a calculated formula of $[Ca_{0.71}Al_{0.29}(OH)_2]$ $(C_{11}H_{15}O_2)_{0.29}\cdot 0.42\ H_2O$ gives 29.5% C, 5.5% H, 40.0% mass of adamantanecarboxylate and 5.8% structural water (mass loss between 100–220 °C in TGA). This is in good agreement with both the experimental and TGA data (around 6 wt% mass loss between 100–220 °C, as shown in Fig. S2 in the ESI†). The PXRD pattern of the resultant LDH (Fig. S1a in the ESI†) shows basal reflections at 4.25 (20.74), 8.46 (10.43) and 12.68°2θ (6.97 Å), and the observed d-spacing matches with the reported values of the adamantanecarboxylate intercalated LDHs.[25] The successful formation of LDH and the intercalation of adamantanecarboxylate was further characterized using FTIR spectra, as shown in Fig. S1b (ESI†). The stretching

vibrations of the layered hydroxyls, along with the intercalated water molecules, can be seen as a broad hump centered around 3378 cm^{-1}. The C–H stretching vibrations of the adamantanecarboxylate ring are seen at 2902 and 2848 cm^{-1}. Symmetric and antisymmetric stretching vibrations of the carboxylate group attached to the adamantane ring can be seen at 1400 and 1518 cm^{-1}, respectively.[26] Generally, the successful synthesis of calcium containing LDHs is difficult because the hydroxide form of calcium, *i.e.* $Ca(OH)_2$, is thermodynamically less stable than the other phases such as calcite ($CaCO_3$). Due to this, most of the reported calcium based LDHs are replete with impurities, mainly calcite. In the present case, both PXRD and IR characterizations confirm the phase pure synthesis of Ca–Al-adamantanecarboxylate LDH. It is interesting to observe that the employed co-hydration method facilitates the synthesis of calcium-based LDHs without any impurities. The surface morphology of the resultant Ca–Al-adamantanecarboxylate LDH was characterized by SEM (Fig. 1a and b). This shows the typical hexagonal sheets of several microns in lateral dimension.

The thermal behaviour of Ca–Al LDH was studied using a gravimetric method under a N_2 atmosphere from room temperature to 850 °C (10 °C min^{-1} ramp rate). The sample starts losing mass from room temperature up until around 700 °C (Fig. S2 in the ESI†) and the total mass loss is around 61 wt%. From the empirical formula calculated above, around 77 wt% of mass loss can be expected, assuming the complete elimination of hydroxyl ions, adamantanecarboxylate ion and water molecules, as volatile gasses. The observed mass loss was lower than expected, suggesting incomplete decomposition/transformation of some of the volatile entities in the LDH. It is well established that intercalated water and hydroxyl ions are known to decompose and escape as water vapour below 400 °C.[27] The only other volatile moiety that could be incompletely decomposed/transformed is the adamantanecarboxylate ion in the interlayer, as reported in the literature.[23]

Generally, thermal decomposition of Ca–Al LDH at 700 °C is expected to generate MMOs that have crystalline CaO and an amorphous/metastable aluminium-containing phase. The PXRD pattern of the MMOs generated from the thermal decomposition of the Ca–Al-adamantanecarboxylate LDH at 700 °C under an inert atmosphere (N_2) is shown in Fig. S3 (ESI†). This shows reflections at 3.02 (29.50), 2.69 (33.17), 2.48 (36.12), 2.28 (39.47), 2.08 (43.28), 1.92 (47.28) and 1.41 Å (65.92°2θ). The weak reflections at 2.69 and 2.48 Å match well with those expected for CaO, and all the other reflections match with those of calcium carbonate.[28] The observation of reflections due to $CaCO_3$ is interesting and this could be due to CaO present in the resultant MMOs, being basic in nature, that could have reacted with atmospheric CO_2, leading to the formation of $CaCO_3$. This indicates the robust carbonation nature of the resultant MMOs. The interesting part of the PXRD (Fig. S3†) is the broad hump centered around 20°2θ that does not match with any of the calcium oxide/aluminium oxide phases. On close examination, it can be seen that the position of the peak matches with that of reduced graphitic oxide.[29] The origin of this graphitic carbon peak should be from the intercalated adamantanecarboxylate ion. During thermal decomposition, the adamantanecarboxylate ion has been converted and graphitized, just like many other carbon molecules.[30]

The obtained MMOs sample was further characterized by FTIR and the resultant spectrum is given in Fig. S4 (ESI†). It

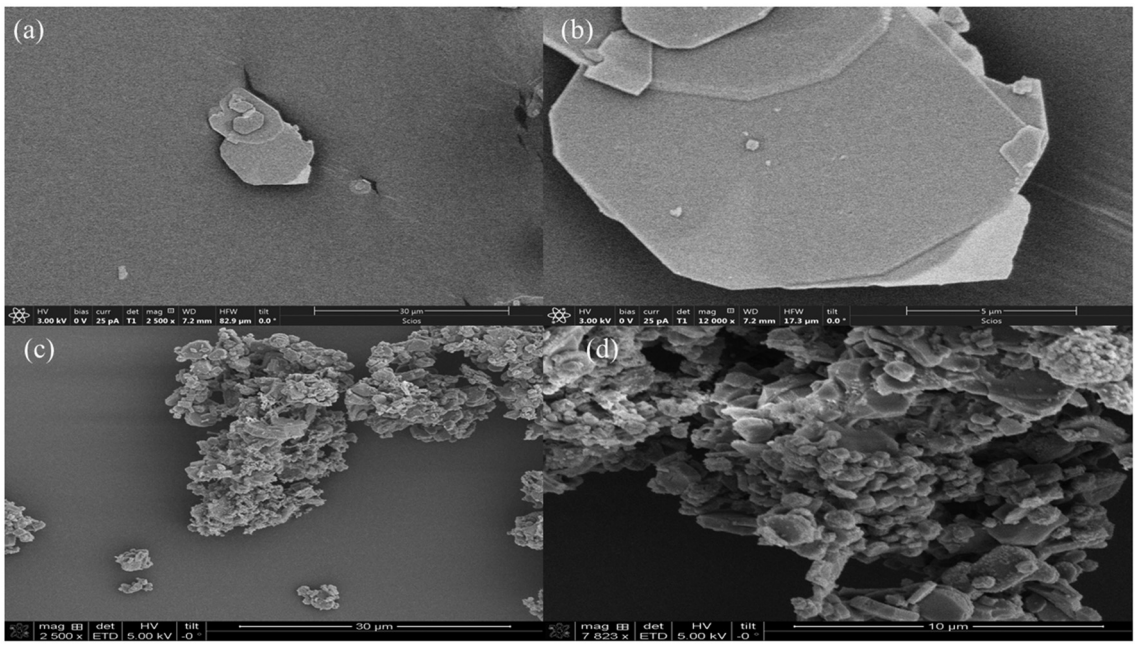

Fig. 1 SEM images of Ca/Al-adamantanecarboxylate LDH (a and b) and the organic–inorganic hybrid MMOs obtained from decomposition of Ca/Al-adamantanecarboxylate LDHs (c and d).

shows the strong stretching vibration at 1410 cm^{-1}, corresponding to metal carbonates and this further confirms the rapid carbonation nature of the MMOs.[26] Due to the high intensity of metal carbonate vibrations, the rest of the spectrum appears featureless at the higher wavenumber region. The enlarged part of the spectrum shown in the inset of Fig. S4 (ESI†) shows a broad hump around 3392 cm^{-1}, indicating the presence of hydroxyl ions. In addition, two small peaks at 2905 and 2850 cm^{-1} are also seen and can be assigned to a C–H vibration of the hydrocarbon moiety originating from the intercalated anion.[31] Small intensity peaks around 2500 and 1790 cm^{-1} fall under the OH and CO stretching vibration regions of the carboxylic acid, respectively.[31] The medium intensity vibration at 780 cm^{-1} falls under the metal–oxygen stretching region.

The origin of the carbon in the resultant MMOs was further characterized by Raman spectroscopy (Fig. 2). This shows characteristic G and D bands for carbon compounds at 1589 and 1356 cm^{-1}, respectively. The intensity of the G band is larger than that of the D band, indicating the nature of the carbon being that of reduced graphite oxide rather than graphite oxide.[32] The Raman spectra also confirmed the presence of the carbon in the resultant MMOs.

The surface area, pore size and pore volume of the resultant MMOs were studied using nitrogen adsorption at 77 K. The adsorption/desorption profile of the resultant MMOs shows a type IV isotherm (Fig. S5a in the ESI†). This shows a BET surface area of 59.5 $m^2\ g^{-1}$, which is much higher than that of the average surface area reported for calcium oxide-based sorbents.[33] The pore volume (0.087 $cm^3\ g^{-1}$) and pore size distribution were calculated using the desorption branch of the isotherm by employing the BJH method. The resultant MMOs shows a pore size distribution of between 8–60 Å, with an average pore size being 20 Å (Fig. S5b in the ESI†). The morphology of the resultant MMOs shows two different kinds of particles (Fig. 1c and d) where small-interconnected particles sit on the large hexagonal sheet-like particles. The small particles could be due to MMOs and the large sheet-like ones could be due to carbon. To verify this, EDX analysis on these two types of particles was conducted (as shown in Fig. S6†).

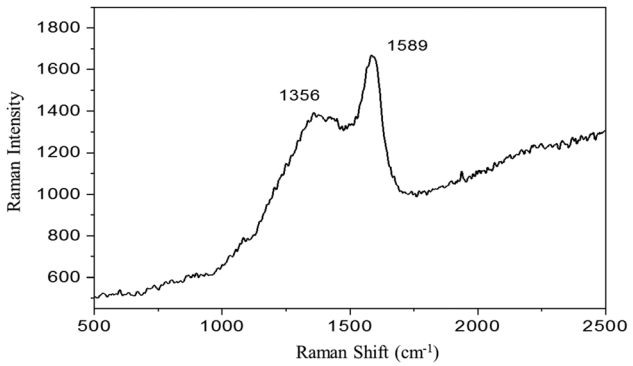

Fig. 2 Raman spectrum of the organic–inorganic hybrid MMOs obtained from decomposition of Ca/Al-adamantanecarboxylate LDH.

The EDX spectra for both the sheet-like particles and the smaller particles showed all the elements (C, O, Al and Ca), indicating the presence of both carbon and the MMOs. However, the percentage of carbon in the sheet-like particles was higher (Fig. S6b†) than that observed in the smaller particles (Fig. S6c†). The fact that the micron-sized large hexagonal sheets contain a higher amount of carbon could be derived from the transformation of the intercalated adamantanecarboxylate ions. The smaller nanoparticles that have greater amounts of Ca and Al are mainly attributed to the MMOs resulting from the layered hydroxides. This thermal behaviour of Ca–Al-adamantanecarboxylate LDH under an inert atmosphere is similar to that proposed in Scheme 1.

The elemental analysis of the resultant MMOs was carried out using the energy dispersive X-ray spectroscopy (EDX) technique (Fig. S7 in the ESI†). The calculated composition of the oxide residue from EDX shows around 30 wt% carbon, 32 wt% oxygen, 27 wt% calcium and 9.5 wt% aluminium. The presence of the carbon in the sample is unusual for LDH-based MMOs. The only source of carbon in the entire LDH is from the adamantanecarboxylate ion. EDX provides additional evidence for the incomplete decomposition/transformation of the intercalated anion. The amount of aluminium is slightly less than expected and it is likely that it has segregated upon thermal decomposition. A bright field TEM image of the resultant MMOs is given in Fig. 3a and b, which shows the sheet-like material having a 5–10 μm lateral dimension. This is similar to the morphology observed in the SEM image, as shown above (Fig. 1c and d). HRTEM images (Fig. 3c) show the organic–inorganic composite type of the MMOs, where both carbon and the metal oxide are clearly visible. The resultant composite shows a structure that is similar to layered materials that have layers of different components, *i.e.* MMOs and the carbon are alternating with each other, as seen in the HRTEM images. Fig. 3d shows the electron diffraction pattern of the resultant MMOs. The results from PXRD, IR, microscopy and EDX conclusively show that 1-adamantanecarboxylate intercalated Ca–Al LDH transformed into an organic–inorganic type of composite under controlled decomposition. The intercalated adamantanecarboxylate ion has transformed into a sheet-like carbon, supporting the oxides of calcium and aluminium, as expected.

High temperature CO_2 capture studies of the developed organic–inorganic composite

The resultant organic–inorganic composite is expected to act as a novel and improved sorbent for high temperature CO_2 capture due to: (a) it having a high surface area compared to similar sorbents and (b) the MMOs being supported on a large sheet of carbon, providing both thermal and mechanical stability. At the same time, the supported carbon sheet can help in the distribution of the active sorbent, CaO. The presence of amorphous aluminium containing phases in the MMOs is known to act as a support for the active sorbents. There is no known evidence of direct aluminium participation in CO_2 capture by MMOs derived from LDHs.[34] In the present case,

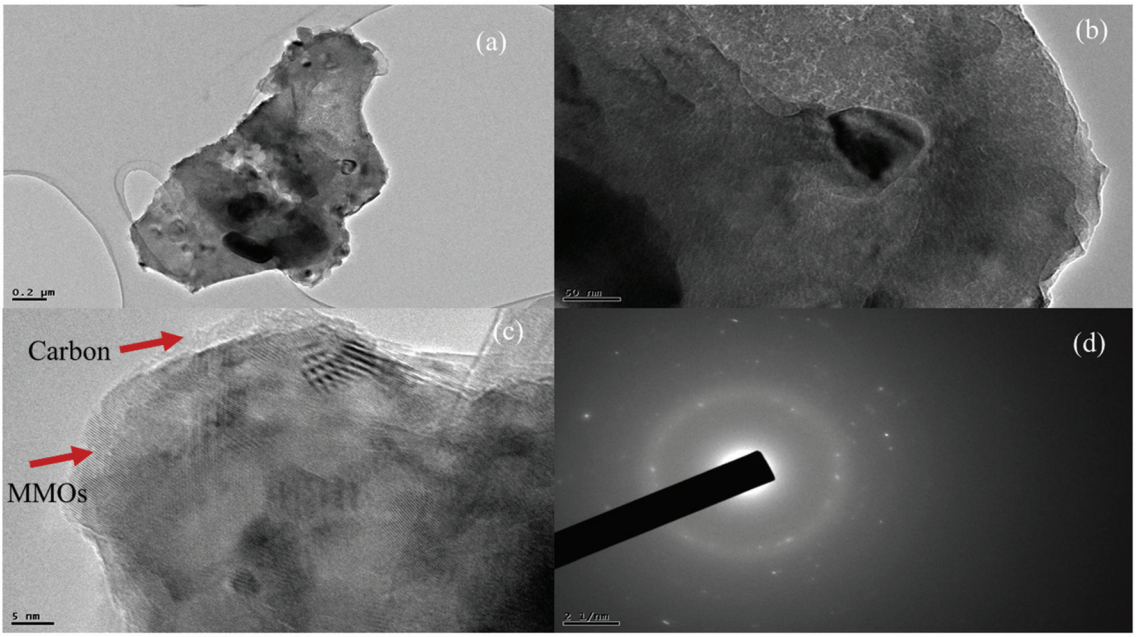

Fig. 3 Bright field TEM images (a and b), HRTEM image (c), and (d) the electron diffraction pattern of the organic–inorganic hybrid MMOs obtained from decomposition of Ca/Al adamantanecarboxylate LDHs.

aluminium containing phases are expected to provide additional support to CaO, along with the residual carbon. The resultant composite is expected to facilitate easy accessibility/diffusion for CO_2 to the active phase, CaO, and thereby improves the overall capture performance of the material. In order to identify the optimum temperature for CO_2 capture for the resultant composite, capture studies were carried out from 200 to 700 °C using TGA (86% CO_2, 14% N_2, 100 mL min^{-1} flow rate). The results are tabulated as shown in Table 1. The sample shows increasing CO_2 adsorption capacity from 200 to 600 °C (from 1.31 mmol g^{-1} to 6.18 mmol g^{-1}, respectively). The adsorption capacity starts decreasing above 600 °C. The sample shows a CO_2 capture capacity of 5.18 and 4.9 mmol g^{-1} at 650 and 700 °C, respectively. The CaO-based sorbents are known to show maximum CO_2 adsorption capacity at 600–650 °C due to maximum carbonation/activation at this temperature.[35] Interestingly, at 600 °C, most of the calcium present in the nanocomposite (~27 wt%, 6.13 mmol g^{-1}) has been carbonated due to the MMOs being highly porous, well-dispersed and supported by the sheet-like carbon. The CO_2

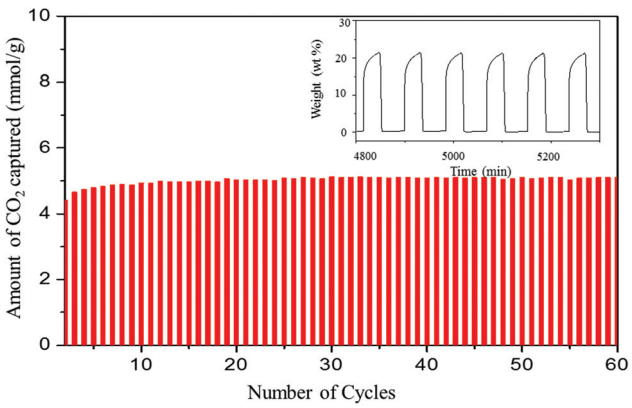

Fig. 4 60 carbonation and regeneration (600 and 700 °C, respectively) cycles of the organic–inorganic hybrid MMOs generated from Ca–Al-adamantanecarboxylate LDHs under 86% CO_2 and 14% N_2. The inset shows the shape and the kinetics of the carbonation/regeneration of the organic–inorganic hybrid MMOs.

Table 1 CO_2 adsorption study of Ca–Al-Ad LDH-based MMOs at different temperatures

Sample	Pre-heating T (°C) (N_2)	Adsorption T (°C) (86% CO_2)	Amount adsorbed (wt %)	Amount adsorbed (mmol g^{-1})
Ca–Al-Ada	700	200	5.7	1.31
Ca–Al-Ada	700	300	8.6	1.95
Ca–Al-Ada	700	600	27.2	6.18
Ca–Al-Ada	700	650	22.8	5.18
Ca–Al-Ada	700	700	21.5	4.90

Ad, adamantanecarboxylate, T, temperature.

uptake values show the near 100% carbonation of all the calcium present in the sample.

Conventionally, the complete regeneration of calcium oxide sorbents is carried out at 900–950 °C, which leads to a very high energy-intensive process.[36] In order to see the regeneration of the developed nanocomposite (under N_2), the regeneration studies were performed at different temperatures, namely 700, 800 and 900 °C. It was found that the resultant nanocomposite sorbent completely regenerated at 700 °C.

The high temperature CO_2 cycling performance of the resultant nanocomposite was determined between 600 (carbonation) and 700 °C (regeneration) for 60 cycles (86% CO_2), as described in the Experimental section. The results of the cycling study are presented in Fig. 4. The sample shows remarkable cyclic stability with nearly 100% regeneration of the sorbent within 30 min of regeneration time. The sample shows an overall working capacity of 5.10 mmol g^{-1} compared to the adsorption capacity of 6.18 mmol g^{-1} in the first cycle. A few cycling data are given in the inset of Fig. 4 to show the stability of the carbonation/regeneration of the sample. The carbonation of the resultant nanocomposite is very rapid and close to 90% of carbonation happens within the first 5 min of the cycle (Fig. S8†). However, the complete regeneration is achieved in less than 5 min, as is evident in Fig. S8.† To check the effect of cycling on the sample and its morphology, as well as the role of the carbon support, SEM was carried out on the cycled nanocomposite (60 cycles). After 60 cycles, the resultant nanocomposite practically retains its original morphology, having its porosity intact, as shown in Fig. 6. The observations of better cycling and retention of the morphology are very interesting results. The presence of carbon in between the MMOs in the nanocomposite has prevented agglomeration/sintering of the particles during the cycling and has hence helped in retaining its capture capacity over long cycles. To employ these sorbents on an industrial scale, it is important to check their activity and cycling stability under flue gas CO_2 concentration. The resultant nanocomposite was tested for capture and cycling stability for 40 carbonation/regeneration cycles under flue gas CO_2 concentration (gas composition of 14% CO_2 and 86% N_2) whilst keeping all other experimental conditions identical to those described in the Experimental section. The results of the cycling performance under flue gas conditions are shown in Fig. 5. The developed nanocomposite shows similar cycling stability to the case of 86% CO_2, except that the cycling capacity has decreased from 5.10 to 4.10 mmol

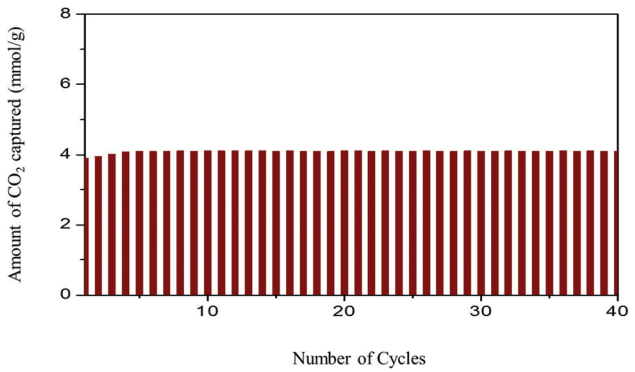

Fig. 5 40 carbonation and regeneration (600 and 700 °C, respectively) cycles of the organic–inorganic hybrid MMOs generated from Ca–Al-adamantanecarboxylate LDHs under 14% CO_2 and 86% N_2.

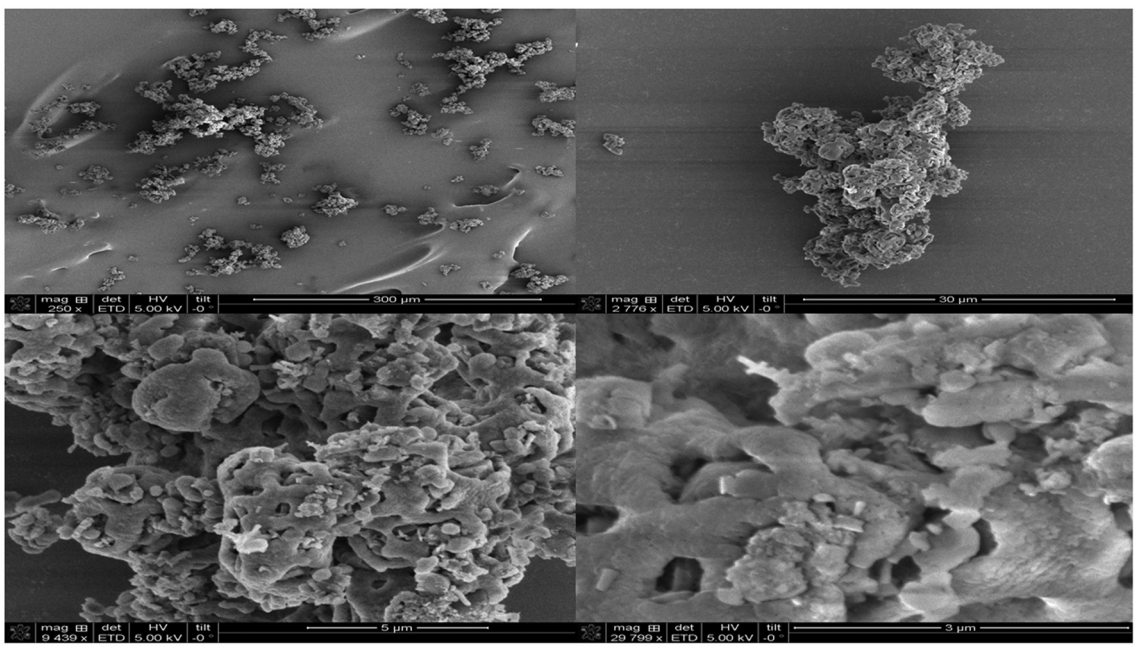

Fig. 6 SEM images after 60 carbonation/regeneration cycles of the organic–inorganic hybrid MMOs generated from Ca–Al-adamantanecarboxylate LDHs.

g^{-1}. This decrease in capture capacity under 14% CO_2 compared to 86% is expected, as the partial pressure of the CO_2 is known to affect the capture capacity. Overall, the resultant organic–inorganic nanocomposite shows excellent CO_2 capture and cycling stability under both CO_2 rich and lean (flue gas) conditions.

4. Conclusions

The layer-interlayer chemistry of LDHs offers ample opportunity to develop MMOs with novel properties. The choice of the intercalated anion is a crucial first step in realizing the novel supported MMOs. Anions that have higher thermal stability and a polymerizable nature need to be intercalated in order to retain/polymerize them during thermal decomposition. The Ca–Al adamantanecarboxylate LDH was synthesized by employing an eco-friendly co-hydration method. The synthesis method utilizes just a stoichiometric amount of chemicals and avoids the excess use of chemicals and post synthesis washing steps. The employed synthesis method facilitates the synthesis of Ca-based LDH without impurities. The as-synthesized Ca–Al-adamantanecarboxylate LDH was successfully converted into a carbon supported MMOs under controlled decomposition in an inert atmosphere. The intercalated adamantanecarboxylate has been transformed to a carbonaceous support for the resultant MMOs leading to the formation of novel organic–inorganic composites. The resultant novel organic–inorganic composite shows excellent CO_2 capture and cycling stability at high temperatures under both CO_2 rich and lean conditions. The amount of CO_2 captured is equivalent to the amount of calcium present in the sample, leading to maximum atom efficiency.

Conflicts of interest

There are no conflicts of interest to declare.

Acknowledgements

We greatly acknowledge Prof. Chris Greenwell, Dept. of Earth Sciences, University of Durham Durham, UK, for helping to record the Raman spectra of the samples. We thank Prof. Berend Smit, Ecole Polytechnique Federale de Lausanne, Switzerland, for his useful comments on the manuscript. We also greatly acknowledge the financial support from the EPSRC through grant EP/N024540/1.

References

1 Global warming of 1.5 °C 2018, an IPCC special report on the impacts of global warming of 1.5 °C above pre-industrial levels and related global greenhouse gas emission pathways, in the context of strengthening the global response to the threat of climate change, sustainable development, and efforts to eradicate poverty.
2 P. M. Cox, R. A. Betts, C. D. Jones, S. A. Spall and I. J. Totterdell, *Nature*, 2000, **408**, 184–187.
3 N. V. D. Assen, P. Voll, M. Peters and A. Bardow, *Chem. Soc. Rev.*, 2014, **43**, 7982–7994.
4 K. Christopher and R. Dimitrios, *Energy Environ. Sci.*, 2012, **5**, 6640–6651.
5 P. Markewitz, W. Kuckshinrichs, W. Leitner, J. Linssen, P. Zapp, R. Bongartz, A. Schreiber and T. E. Müller, *Energy Environ. Sci.*, 2012, **5**, 7281–7305.
6 (*a*) J. C. Abanades, E. S. Rubin, M. Mazzotti and H. J. Herzog, *Energy Environ. Sci.*, 2017, **10**, 2491–2499; (*b*) M. T. Dunstan, A. Jain, W. Liu, S. P. Ong, T. Liu, J. Lee, K. A. Persson, S. A. Scott, J. S. Dennis and C. P. Grey, *Energy Environ. Sci.*, 2016, **9**, 1346–1360.
7 G. T. Rochelle, *Science*, 2009, **325**, 1652–1654.
8 B. Dutcher, M. Fan and A. G. Russell, *ACS Appl. Mater. Interfaces*, 2015, **7**, 2137–2148.
9 (*a*) A. Samanta, A. Zhao, G. K. H. Shimizu, P. Sarkar and R. Gupta, *Ind. Eng. Chem. Res.*, 2012, **51**, 1438–1463; (*b*) J. Wang, L. Huang, R. Yang, Z. Zhang, J. Wu, Y. Gao, Q. Wang, D. O'Hare and Z. Zhong, *Energy Environ. Sci.*, 2014, **7**, 3478–3518; (*c*) D. M. D'Alessandro, B. Smit and J. R. Long, *Angew. Chem., Int. Ed.*, 2010, **49**, 6058–6082; (*d*) K. Adil, P. M. Bhatt, Y. Belmabkhout, S. M. T. Abtab, H. Jiang, A. H. Assen, A. Mallick, A. Cadiau, J. Aqil and M. Eddaoudi, *Adv. Mater.*, 2017, **29**, 1702953.
10 Y. S. Bae and R. Q. Snurr, *Angew. Chem., Int. Ed.*, 2011, **49**, 11586–11596.
11 Q. Wang, J. Luo, Z. Zhong and A. Borgna, *Energy Environ. Sci.*, 2011, **4**, 42–55.
12 (*a*) M. Pérez-Fortes, J. A. Moya, K. Vatopoulos and E. Tzimas, *Energy Procedia*, 2014, **63**, 6534–6543; (*b*) D. Leesona, N. Mac Dowell, N. Shaha, C. Petit and P. S. Fennell, *Int. J. Greenhouse Gas Control*, 2017, **61**, 71–84; (*c*) M. C. Romanoa, R. Anantharaman, A. Arasto, D. C. Ozcan, H. Ahn, J. W. Dijkstra, M. Carbo and D. Boavida, *Energy Procedia*, 2013, **37**, 7176–7185.
13 S. Choi, J. H. Drese and C. W. Jones, *ChemSusChem*, 2009, **2**, 796–854.
14 J. Wang, Y. Zhang, N. Altaf, D. O'Hare and Q. Wang, Layered Double Hydroxides derived Intermediate temperature CO2 Adsorbents, in *Inorganic Materials Series No. 1 Pre-combustion Carbon Dioxide Capture Materials*, ed. Q. Wang, The Royal Society of Chemistry, 2018, pp. 1–60.
15 X. Duan and D. G. Evans, Layered double hydroxides, in *Struct. Bonding*, ed. D. M. P. Mingos, Springer-Verlag, Berlin, Heidelberg, 2006, pp. 1–233.
16 F. Cavani, F. Trifiro and A. Vaccari, *Catal. Today*, 1991, **11**, 173–301.
17 V. Rives, Study of Layered Double Hydorxides by thermal methods, in *Layered Double Hydroxides: Present and future*, ed. V. Rives, Nova Science Publisher. Inc., New York, 2001, pp. 127–151.

18 Y. Gao, Z. Zhang, J. Wu, X. Yi, A. Zheng, A. Umar, D. O'Hare and Q. Wang, *J. Mater. Chem. A*, 2013, **1**, 12782–12790.

19 (*a*) Q. Wang, W. Zhihuai, H. T. Hui, C. Luwei, L. Yan, C. Jie, Z. Ziyi, L. Jizhang and A. Borgna, *Catal. Today*, 2011, **164**, 198–203; (*b*) Q. Wang, H. H. Tay, D. J. W. Ng, L. Chen, Y. Liu, J. Chang, Z. Zhong, J. Luo and A. Borgna, *ChemSusChem*, 2010, **3**, 965–973; (*c*) C. T. Yavuz, D. S. Brian, A. V. Iretskii, M. G. White, T. Golden, M. Atilhan, P. C. Ford and D. G. Stucky, *Chem. Mater.*, 2009, **21**, 3473–3475.

20 G. V. Manohara, *RSC Adv.*, 2014, **4**, 46126–46132.

21 (*a*) M. K. Ram Reddy, Z. P. Xu, G. Q. Lu (Max) and J. C. Diniz da Costa, *Ind. Eng. Chem. Res.*, 2008, **47**, 2630–2635; (*b*) A. Garcia-Gallastegui, D. Iruretagoyena, M. Mokhtar, A. M. Asiri, S. N. Basahel, S. A. Al-Thabaiti, A. O. Alyoubi, D. Chadwick and M. S. P. Shaffer, *J. Mater. Chem.*, 2012, **22**, 13932–13940; (*c*) A. Garcia-Gallastegui, D. Iruretagoyena, V. Gouvea, M. Mokhtar, A. M. Asiri, S. N. Basahel, S. A. Al-Thabaiti, A. O. Alyoubi, D. Chadwick and M. S. P. Shaffer, *Chem. Mater.*, 2012, **24**, 4531–4539; (*d*) J. Wang, L. A. Stevens, T. C. Drage and J. Wood, *Chem. Eng. Sci.*, 2012, **68**, 424–431; (*e*) A. D. Ebner, S. P. Reynolds and J. A. Ritter, *Ind. Eng. Chem. Res.*, 2006, **45**, 6387–6392; (*f*) O. Aschenbrenner, P. McGuire, S. Alsamaq, J. Wang, S. Supasitmongkol, B. Al-Duri, P. Styring and J. Wood, *Chem. Eng. Res. Des.*, 2011, **89**, 1711–1721.

22 (*a*) J. Zhang, Y. Feng, H. Ishiwata, Y. Miyata, R. Kitaura, J. E. P. Dahl, R. M. K. Carlson, H. Shinohara and D. Tománek, *ACS Nano*, 2012, **6**, 8674–8683; (*b*) Y. Feng, H. Ishiwata, Y. Miyata, R. Kitaura, J. E. P. Dahl, R. M. K. Carlson, N. A. Fokina, P. R. Schreiner, D. Tománek and H. Shinohara, *Angew. Chem., Int. Ed.*, 2013, **52**, 3717–3721.

23 G. V. Manohara, H. C. Greenwell, G. S. Alabedi, J. A. Hall and A. Whiting, US20170266642A1, 2017.

24 M. Ogawa and S. Asai, *Chem. Mater.*, 2000, **12**, 3253–3255.

25 G. V. Manohara, Li Li, A. Whiting and H. C. Greenwell, *Dalton Trans.*, 2018, **47**, 2933–2938.

26 K. Nakamota, *Infrared and Raman spectroscopy of inorganic and coordination compounds*, Wiley, New York, 1986.

27 J. Pérez-Ramírez, G. Mul, F. Kapteijn and J. A. Moulijn, *J. Mater. Chem.*, 2001, **11**, 821–830.

28 (*a*) E. A. Harrington, *Am. J. Sci.*, 1927, **13**, 477; (*b*) J. D. Hanawalt, H. W. Rinn and L. K. Frevel, *Ind. Eng. Chem., Anal. Ed.*, 1938, **10**, 457–512.

29 Y. J. Oh, J. J. Yoo, Y. I. Kim, J. K. Yoon, H. N. Yoon, J. H. Kim and S. B. Park, *Electrochim. Acta*, 2014, **116**, 118–128.

30 J. Tang, R. R. Salunkhe, J. Liu, N. L. Torad, M. Imura, S. Furukawa and Y. Yamauchi, *J. Am. Chem. Soc.*, 2015, **137**, 1572–1580.

31 E. Pretsch, P. Buhlmann and M. Badertscher, *Structure Determination of Organic Compounds*, Springer-Verlag, Berlin Heidelberg, 2009.

32 A. K. Das, M. Srivastav, R. K. Layek, M. E. Uddin, D. Jung, N. H. Kim and J. H. Lee, *J. Mater. Chem. A*, 2014, **2**, 1332–1340.

33 (*a*) M. Broda, A. M. Kierzkowska and C. R. Müller, *Adv. Funct. Mater.*, 2014, **24**, 5753–5761; (*b*) N. J. Amos, M. Widyawati, S. Kureti, D. Trimis, A. I. Minett, A. T. Harris and T. L. Church, *J. Mater. Chem. A*, 2014, **2**, 4332–4339; (*c*) Z. Zhou, Y. Qi, M. Xie, Z. Cheng and W. Yuan, *Chem. Eng. Sci.*, 2012, **74**, 172–180.

34 G. Hu, L. Zhu, A. Jia, X. Hu, G. Xie, J. Lu and M. Luo, *Appl. Spectrosc.*, 2012, **66**, 122–127.

35 A. Armutlulu, M. A. Naeem, L. Hsueh-Ju, S. M. Kim, A. Kierzkowska, A. Fedorov and C. R. Müller, *Adv. Mater.*, 2017, **29**, 1702896.

36 W. Wang, S. Ramkumar and F. Liang-Shih, *Fuel*, 2013, **104**, 561–574.